

False Vacuum Lumps with Fermions

Ramin G. Daghigh

Physics Department, University of Winnipeg, Winnipeg, Manitoba R3B 2E9, Canada

Abstract

This paper studies false vacuum lumps surrounded by the true vacuum in a real scalar field potential in flat spacetime. Fermions reside in the core of the lump, which are coupled with the scalar field via Yukawa interaction. Such lumps are stable against spherical collapse and deformation from spherical shape based on energetics considerations. The fermions inside the lump are treated as a uniform Fermi gas. We consider the Fermi gas in both ultrarelativistic and nonrelativistic limits. The mass and size of these lumps depend on the scale characterizing the scalar field potential as well as the mass density of the fermions.

1. Introduction

The spacetime geometry of gravitating lumps is either anti-de Sitter-Schwarzschild or de Sitter-Schwarzschild. Dymnikova has discussed the global structure of de Sitter-Schwarzschild spacetime, supposing appropriate external matter distribution [1]. The spacetime geometry of the gravitating fermionic lumps in Ref. [2] is anti-de Sitter-Schwarzschild. The mass of such lumps is negative. In this paper we shall investigate fermionic lumps with positive mass in flat spacetime. The equations in flat spacetime become simple and we expect to obtain similar solutions in curved spacetime where the geometry is de Sitter-Schwarzschild. The exploration of the de Sitter-Schwarzschild spacetime is reserved for future investigation. One may explore such objects in the universe at various scales and epochs.

In field theories with continuous global symmetries, non-dissipative solutions with finite energy may exist. These solutions are called non-topological solitons [3, 4, 5]. The model studied in this paper is very similar to a kind of non-topological soliton called Fermi balls, given in Ref. [6]. In Fermi balls, fermions have zero rest mass and their effective mass is due to their Yukawa coupling with a scalar field. In such a model, fermions energetically have a tendency to localize at the boundary wall region (domain wall) where their effective mass becomes zero. In our model, however, fermions have a nonzero rest mass and their effective mass reaches a minimum at the core region of the lump causing the fermions to localize at this region.

In section 2, we set up the problem and introduce useful variables in terms of which the field equations are written. In section 3, we investigate the stability of the lumps with a positive mass analytically. In section 4, the behavior of the solutions is investigated analytically inside the lump, numerically in the boundary wall region, and analytically outside the lump. More details of the solutions are given in section 5, with a focus on the dependence of the solutions on various parameters of the model. It is seen how the solutions change as the energy scale of the model is lowered. In Section 6, we investigate the numerical solutions in the transition region with the fermion density having a continuous transition to zero. The summary and conclusions are given in Section 7.

2. Model with Dirac fermions

The system that we are considering is a real scalar field coupled with a fermion field whose Lagrangian is given by

$$\mathcal{L} = i\bar{\psi}\gamma^\mu\partial_\mu\psi - m\bar{\psi}\psi + \frac{1}{2}\partial^\mu\phi\partial_\mu\phi - V[\phi] - g\phi\bar{\psi}\psi . \quad (2.1)$$

We take

$$V[\phi] = \frac{\lambda}{4}(\phi - f_2)\left\{\phi^3 - \frac{1}{3}(f_2 + 4f_1)\phi^2 - \frac{1}{3}f_2(f_2 - 2f_1)(\phi + f_2)\right\} . \quad (2.2)$$

This potential has two non-degenerate minima at f_1 and f_2 . For further details on the potential refer to Ref. [2]. In this paper, we employ the natural unit $\hbar = c = 1$.

As we shall see below, the scalar field ϕ is approximately constant inside the lump so that fermions inside the lump may be treated as a uniform Fermi gas. The effective mass of the fermion is $m_{\text{eff}} = m + g\phi_{\text{inside}}$. Depending on the density ρ_n and effective mass m_{eff} of fermions, the Fermi gas can be either relativistic or nonrelativistic. Given ρ_n and m_{eff} , $\langle\bar{\psi}\psi\rangle = \rho_0$ inside the lump is determined. Let p_F be the Fermi momentum of a degenerate Fermi gas. Then

$$\begin{aligned} \rho_n &= \frac{p_F^3}{3\pi^2} , \\ \rho_0 &= \frac{m_{\text{eff}}}{2\pi^2}\left\{p_F(p_F^2 + m_{\text{eff}}^2)^{1/2} - m_{\text{eff}}^2 \log \frac{p_F + (p_F^2 + m_{\text{eff}}^2)^{1/2}}{m_{\text{eff}}c}\right\} . \end{aligned} \quad (2.3)$$

Note that $\rho_0 \sim \rho_n$ if fermions are nonrelativistic. The energy-momentum tensors $T_{\mu\nu}$ for spherically symmetric, static configurations are

$$\begin{aligned} T_{00} &= \frac{1}{2}\phi'^2 + V[\phi] + \mathcal{E}_f , \\ T_{11} &= \frac{1}{2}\phi'^2 - V[\phi] + P_f , \\ T_{22} = T_{33} &= -\frac{1}{2}\phi'^2 - V[\phi] + P_f , \\ \text{others} &= 0 , \end{aligned} \quad (2.4)$$

where primes represent r derivatives. Here

$$\mathcal{E}_f = \frac{1}{8\pi^2}\left\{p_F(2p_F^2 + m_{\text{eff}}^2)(p_F^2 + m_{\text{eff}}^2)^{1/2} - (m_{\text{eff}})^4 \log \left[\frac{p_F + (p_F^2 + m_{\text{eff}}^2)^{1/2}}{m_{\text{eff}}}\right]\right\} , \quad (2.5)$$

and

$$P_f = \frac{1}{8\pi^2} \left\{ p_F \left(\frac{2}{3} p_F^2 - m_{\text{eff}}^2 \right) (p_F^2 + m_{\text{eff}}^2)^{1/2} + (m_{\text{eff}})^4 \log \left[\frac{p_F + (p_F^2 + m_{\text{eff}}^2)^{1/2}}{m_{\text{eff}}} \right] \right\} \quad (2.6)$$

are the energy density and the pressure density of a Fermi gas, respectively. T_{00} is the energy density of the lump which can be used to calculate the total mass of the lump

$$M = \int_0^r 4\pi r^2 dr T_{00} \quad . \quad (2.7)$$

The equation of motion for the scalar field is

$$-\frac{1}{r^2} \frac{\partial}{\partial r} (r^2 \phi') + V'[\phi] + g\rho_S(r) = 0 \quad (2.8)$$

where $\rho_S(r) = \langle \bar{\psi} \psi \rangle(r)$, and $V'[\phi]$ is the derivative of $V[\phi]$ with respect to ϕ .

In order to solve Eq. (2.8) we adopt an approximation

$$\rho_S(r) = \rho_0 \theta(R_1 - r) \quad , \quad (2.9)$$

and we divide the space into three regions:

- I. The inside region ($0 \leq r \leq R_1$).
- II. The boundary wall region ($R_1 \leq r \leq R_2$).
- III. The outside region ($R_2 \leq r < \infty$).

In region I inside the lump, $\rho_S = \rho_0$ and $\phi(0)$ is very close to, but still greater than the location f_S of the minimum of $V[\phi] + g\phi\rho_0$: $\phi(0) = f_S + \delta\phi(0)$ with $0 < \delta\phi(0)/|f_S| \ll 1$. In the inside region, $\phi(r)$ varies little from f_S so that the equation of motion for ϕ can be linearized. In region II, $\rho_S = 0$. In this region the field varies substantially and the full nonlinear equation must be solved numerically. In region III, $\rho_S = 0$ and $\phi \sim f_2$. In this paper we focus on the case in which $|f_1| \sim f_2 \sim f \equiv \frac{1}{2}(|f_1| + f_2)$, $f_r = (f_2 - |f_1|)/f \ll 1$ and $f_1 - f_S \ll f$ so that the linearization of Eq. (2.8) is valid. In Section 6, we will relax the third restriction by using a continuous transition from $\rho_S = \rho_0$ to $\rho_S = 0$ in region II. Schematic behavior of a solution $\phi(r)$ is displayed in Fig. 1.

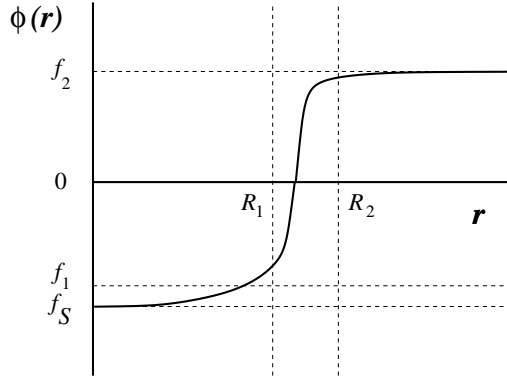


Figure 1: Schematic behavior of $\phi(r)$. In the lump solutions $|f_1 - f_S| \ll |f_1|$ and $R_2 - R_1 \ll R_1$.

3. Stability of lumps

As we mentioned earlier, the scalar field inside the lump (region I) is approximately constant. This allows us to treat the fermions inside the lump as a uniform Fermi gas. In this region, the Yukawa interaction $g\phi\bar{\psi}\psi$ generates an additional linear interaction $g\rho_0\phi$ for the scalar field. The total potential $V[\phi] + g\rho_0\phi$ has a minimum at $f_S < 0$. Let R be the radius of the lump. To see how false vacuum lumps with fermions become possible from energetics considerations, we suppose that the total fermion number $N_F = 4\pi R^3 \rho_n/3$ is conserved and therefore fixed. It is supposed that $V[f_1] \equiv \epsilon_0 > 0$ but the energy density at the minimum $V[f_S] + g\rho_0 f_S = \epsilon$ becomes negative for the lump solution. f_S and ϵ depend on ρ_n or R . Inside the lump $r < R$, the scalar field assumes $\phi \sim f_S$ whereas outside the lump $\phi = f_2$. The total energy of the lump is approximately given by

$$E(R) = \left\{ \mathcal{E}_f(\rho_n, m_{\text{eff}}) + \epsilon(\rho_0) \right\} V + S\sigma + E_{f,\text{wall}}(R), \quad (3.1)$$

where σ is the surface tension resulting from varying ϕ in the boundary wall region. $V = 4\pi R^3/3$ and $S = 4\pi R^2$ are the volume and the surface area of the lump, respectively. $\rho_0 = \rho_0(\rho_n, m_{\text{eff}})$ as related by (2.3). The energy density of a degenerate Fermi gas $\mathcal{E}_f(\rho_n, m_{\text{eff}})$ is given in (2.5). $E_{f,\text{wall}}(R)$ is the contribution to the energy from fermions localized in the boundary wall region. $E_{f,\text{wall}}(R)$ has been estimated in Ref. [7] to be about $4\sqrt{\pi} N_{f,\text{wall}}^{3/2}/3\sqrt{S}$ for $m = 0$, where $N_{f,\text{wall}}$ is the number of fermions confined in the boundary wall region. In this paper, we shall focus on the case $N_{f,\text{wall}} \ll N_F$.

Using Eq. (2.5), the energy density of a degenerate Fermi gas can be found in the nonrelativistic limit where $p_F \ll m_{\text{eff}}$, and in the ultrarelativistic limit where $p_F \gg m_{\text{eff}}$.

In the nonrelativistic limit

$$\mathcal{E}_f \approx m_{\text{eff}} \rho_n + \frac{A}{m_{\text{eff}}} \rho_n^{5/3}, \quad (3.2)$$

where $A = 3(3\pi^2)^{2/3}/10$, and in the ultrarelativistic limit

$$\mathcal{E}_f \approx B \rho_n^{4/3}, \quad (3.3)$$

where $B = (9\pi)^{2/3}/4$.

For fixed N_F , $\epsilon(\rho_0) \sim \epsilon_0$ for $\rho_n \sim 0$ (as $R \rightarrow \infty$). Therefore, $E(R) \sim (4\pi\epsilon_0/3)R^3$ for large R in both nonrelativistic and ultrarelativistic cases. For large ρ_n (as $R \rightarrow 0$), the total potential is approximated by $(\lambda/4)\phi^4 + g\rho_n\phi$ near the minimum so that $\epsilon \sim -\frac{3}{4}\lambda^{-1/3}(g\rho_n)^{4/3}$. In the case of a lump with a nonrelativistic Fermi gas the \mathcal{E}_f -term dominates over the ϵ -term for small R and $E(R) \sim A'R^{-2}$, where $A' > 0$. On the other hand, for a lump with an ultrarelativistic Fermi gas the \mathcal{E}_f -term can only dominate over the ϵ -term for small R if $B > \frac{3}{4}\lambda^{-1/3}g^{4/3}$ or

$$\frac{g^4}{\lambda} > 3\pi^2. \quad (3.4)$$

If Eq. (3.4) is satisfied, then $E(R) \sim B'R^{-1}$ with $B' > 0$. Therefore, with Eq. (3.4) satisfied, the total energy $E(R)$ of a false vacuum lump filled with either ultrarelativistic or nonrelativistic Fermi gas has a minimum at a certain radius \bar{R} , where \bar{R} is the size of the lump.

Now let us explore some of the conditions and restrictions on the lump solutions in this paper. For the lump solutions to become possible we need to have $\epsilon < 0$. Note that $\epsilon < 0$ implies that

$$\rho_0 > \frac{\epsilon_0}{gf} \sim \frac{\lambda}{g} f^3 f_r. \quad (3.5)$$

In the examples of the lump solutions below, f_S is close to f_1 , and it is useful to introduce the parameter $h_S = (f_1 - f_S)/f \ll 1$. ρ_0 and h_S are related by

$$\rho_0 \sim \frac{2\lambda}{g} f^3 h_S. \quad (3.6)$$

Equations (3.5) and (3.6) imply that

$$2h_S > f_r. \quad (3.7)$$

Also in this paper $|\epsilon| \gg \epsilon_0$. In other words

$$|\epsilon| \sim gf\rho_0. \quad (3.8)$$

First we consider a lump filled with nonrelativistic Fermi gas. As we mentioned earlier, the nonrelativistic approximation is justified if $m_{\text{eff}} \gg p_F$, which implies that

$$m_{\text{eff}} \gg \rho_0^{1/3} \sim \left(\frac{\lambda h_S}{g^4}\right)^{1/3} gf . \quad (3.9)$$

We would like to have a lump with positive energy; $\mathcal{E}_f + \epsilon > 0$. This leads to

$$m_{\text{eff}} > \frac{|\epsilon|}{\rho_n} \sim gf . \quad (3.10)$$

If the conditions in Eqs. (3.8) and (3.9) are satisfied, we may have a false vacuum lump filled with nonrelativistic Fermi gas with positive mass. Now let us consider a lump filled with ultrarelativistic Fermi gas. The ultrarelativistic approximation is justified if $m_{\text{eff}} \ll p_F$, which implies that

$$m_{\text{eff}} \ll \rho_0^{1/3} \sim \left(\frac{\lambda h_S}{g^4}\right)^{1/3} gf . \quad (3.11)$$

For this case also we would like to have a lump with positive energy; $\mathcal{E}_f + \epsilon > 0$. This leads to

$$m_{\text{eff}} < \frac{\pi \rho_0}{|\epsilon|^{1/2}} \sim \frac{2\pi \lambda h_S}{g^4} (gf)^{5/2} . \quad (3.12)$$

If the conditions in Eqs. (3.11) and (3.12) are satisfied, we may have a false vacuum lump filled with ultrarelativistic Fermi gas which has a positive mass.

Note that if the fermion rest mass $m \gtrsim gf$, then the effective mass of the fermion inside the lump, which is $|m - gf|$, is smaller than the effective mass of the fermion outside the lump, which is $m + gf$. This condition is satisfied for both cases of lumps with nonrelativistic and ultrarelativistic Fermi gas. This is the reason why fermions energetically favor to reside at the core of the lump. The situation will change when the fermion rest mass $m \ll gf$ or $m = 0$. These scenarios have been studied in the models suggested in Refs. [2] and [6].

The stability of a lump configuration against deformation from spherical shape is examined in the following way. In Eq. (3.1), the surface tension energy and the energy from fermions localized at the boundary region $E_{f,\text{wall}}(R)$ depend only on the surface area of the lump and not on its volume. On the other hand, it is clear from Eqs. (3.1), (3.2), (3.3), and (3.8) that the volume energy will increase if we decrease the volume of the lump by deforming it from spherical shape for both nonrelativistic and ultrarelativistic cases.

4. Behavior of the solutions

The procedure to solve Eq. (2.8) using the assumption described in the previous section is as follows:

Region I

First we determine f_S using

$$V'[f_S] + \rho_0 = 0 \quad . \quad (4.1)$$

f_S and f_1 are close to each other compared to the length scale f . Denoting $\phi(0)$ by ϕ_0 , we have $0 < \phi_0 - f_S \ll |f_S|$.

The equation for $\phi(r)$ can be linearized with $\delta\phi(r) = \phi(r) - f_S$. In terms of $z \equiv r\omega$,

$$\left\{ \frac{d^2}{dz^2} + \frac{2}{z} \frac{d}{dz} - 1 \right\} \delta\phi = 0 \quad , \quad (4.2)$$

where $\omega^2 = V''[f_S]$. The solution to Eq. (4.2) regular at $r = 0$ is

$$\delta\phi(r) = \delta\phi(0) \frac{\sinh z}{z} \quad . \quad (4.3)$$

As one can see, the ratio $\delta\phi(r)/\delta\phi(0)$ grows exponentially as $e^z/2z$. At the end of region I, $\delta\phi/|f_S|$ needs to be very small for the linearization to be valid. The deviation from f_S at the origin, $\delta\phi(0)$, needs to be very small to have an acceptable solution.

The ratio of $\delta\phi'(r)$ to $\delta\phi(r)$ is given by

$$\frac{\delta\phi'(r)}{\delta\phi(r)} = \omega \left(\frac{\cosh z}{\sinh z} - \frac{1}{z} \right) \sim \omega \quad , \quad (4.4)$$

for $z \gg 1$.

Region II

In region II, the equation must be solved numerically because $\phi(r)$ varies significantly. Nontrivial lump solutions become possible by fine tuning the value of $\delta\phi(R_1)$.

How to find the numerical solutions is summarized as follows. First we choose R_1 , $\delta\phi(R_1)$, and f_S . $\delta\phi'(R_1)$ is evaluated from the analytic solution in region I. Using the boundary conditions $\delta\phi(R_1)$ and $\delta\phi'(R_1)$, we solve the equation numerically in this region. The width of the boundary wall region, $w = R_2 - R_1$, is approximately given by $1/\sqrt{\lambda} f$ [8].

One example of the lump solutions in region II is displayed in Fig. 2. In this example, we choose the input parameters $g = 1$, $\lambda = 1$, $f/M_{\text{Pl}} = 0.0002$, $f_r = \Delta f/f = 0.0002$ and

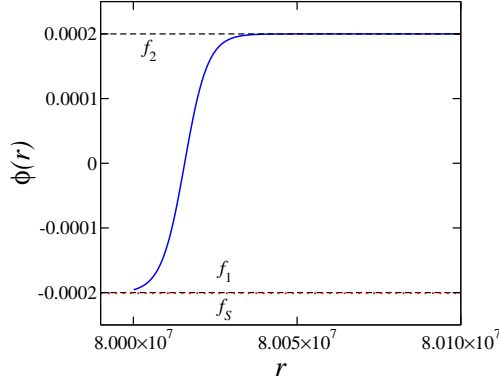


Figure 2: $\phi(r)$ of a solution with $f/M_{\text{Pl}} = 0.0002$, $f_r = 0.0002$, $\lambda = g = 1$, $h_S = (f_1 - f_S)/f = 0.005$ and $R_1/l_{\text{Pl}} = 8 \times 10^7$. ϕ and r are in the units of M_{Pl} and l_{Pl} , respectively.

$h_S = (f_1 - f_S)/f = 0.005$. The resulting output parameters are: $\rho_0 l_{\text{Pl}}^3 = 8.0593 \times 10^{-14}$, $\epsilon/M_{\text{Pl}}^4 = -1.5944 \times 10^{-17}$, $|\epsilon|/\epsilon_0 = 74.738$ and $\omega/M_{\text{Pl}} = 2.8495 \times 10^{-4}$. We note that $\rho_0/f^3 = 0.0101$ and $\epsilon/f^4 = -0.00997$. For $R_1/l_{\text{Pl}} = 8 \times 10^7$ ($R_1\omega = 2.2796 \times 10^4$), we find a solution with $\delta\phi(R_1)/M_{\text{Pl}} = 5.1491304 \dots \times 10^{-6}$. In this example, the value of $\delta\phi$ at the origin ($r = 0$) is found from Eq. (4.3) to be 1.562×10^{-9901} , which explains why one cannot numerically integrate $\phi(r)$ starting from $r = 0$ to R_1 . A small discontinuity in ϕ'' appears at $r = R_1$ due to the discontinuous change in $\rho_S(r)$.

Suppose that the fermion mass is $10^{-3}M_{\text{Pl}}$. Then for the given example above, we have a false vacuum lump filled with nonrelativistic Fermi gas which has a total mass of

$$M \approx \left\{ \epsilon(\rho_n) + m_{\text{eff}}\rho_n + \frac{3(3\pi^2)^{2/3}}{10m_{\text{eff}}} \rho_n^{5/3} \right\} \frac{4\pi R^3}{3} = 1.4 \times 10^8 M_{\text{Pl}}. \quad (4.5)$$

For the same given example, let us take the fermion mass to be $10^{-19}M_{\text{Pl}}$, which is approximately equal to proton mass. In this case, we would have a false vacuum lump filled with ultrarelativistic Fermi gas with a total mass of

$$M \approx \left\{ \epsilon(\rho_0) + \frac{(9\pi)^{2/3}}{4} \rho_n^{4/3} \right\} \frac{4\pi R^3}{3} = 1.4 \times 10^{37} M_{\text{Pl}}. \quad (4.6)$$

In both of these examples, the energy contribution from surface tension σ is small ($\sim 10^6 M_{\text{Pl}}$) and can be ignored.

The behavior of energy density T_{00} is displayed in Fig. 3. The energy density has one sharp peak associated with the rapid variation of ϕ .

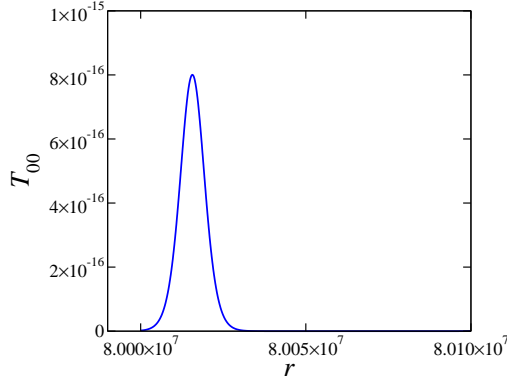


Figure 3: The energy density T_{00} for a solution with $f/M_{\text{Pl}} = 0.0002$, $f_r = 0.0002$, $\lambda = g = 1$, $h_S = (f_1 - f_S)/f = 0.005$ and $R_1/l_{\text{Pl}} = 8 \times 10^7$. T_{00} and r are in the units of M_{Pl}^4 and l_{Pl} , respectively. For $r < R_1$, $T_{00} \sim \epsilon + m\rho_n + \frac{3(3\pi^2)^{2/3}}{10m} \rho_n^{5/3} > 0$.

The field $\phi(r)$ approaches f_2 for $r > R_2$. In the numerical integration, R_1 and f_S are kept fixed while $\delta\phi(R_1)$ is varied. If $\delta\phi(R_1)$ is chosen to be slightly smaller, ϕ comes back toward, but cannot reach f_1 , eventually oscillating around $\phi = 0$ as r increases. If $\delta\phi(R_1)$ is taken to be slightly bigger, then $\phi(r)$ overshoots f_2 , heading for $+\infty$ as r increases. With just the right value, $\phi(r)$ approaches to f_2 as $r \rightarrow \infty$ in region III. Shell solutions can appear in which ϕ goes back to f_1 at $r = \infty$.

Region III

In region III, $\phi(r)$ is very close to f_2 . The equation for $\phi(r)$ can be linearized with $\delta\phi(r) = f_2 - \phi(r)$. The linearized equation is the same as Eq. (4.2) with $z \equiv r\alpha$, where $\alpha^2 = V''[f_2]$. The solution in which $\delta\phi(r \rightarrow \infty) = 0$ is

$$\delta\phi(r) = \delta\phi(R_2) \cdot \frac{e^{-z+z_2}}{z/z_2}. \quad (4.7)$$

The value of $\delta\phi(R_2)$ is determined numerically.

5. Numerical Analysis in the Nonlinear Regime

In the previous section, we solved the field equation in three different regions of space. In this section, we analyze our numerical results in more detail.

The lump solutions depend on several dimensionless parameters of our model such as f/M_{Pl} , f_r , $R_1\omega$, and $\rho_0 f^3$. The dependence on g and λ can be absorbed by rescaling.

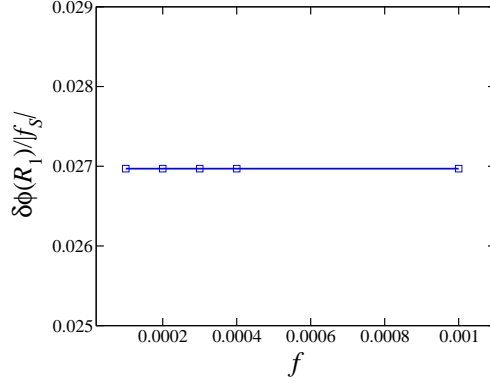


Figure 4: The f dependence of $\delta\phi(R_1)$. $\lambda = g = 1$, $f_r = 0.0002$, $R_1\omega = 2 \times 10^4$ and $h_S = (f_1 - f_S)/f = 0.005$ are fixed. f is in the units of M_{Pl} .

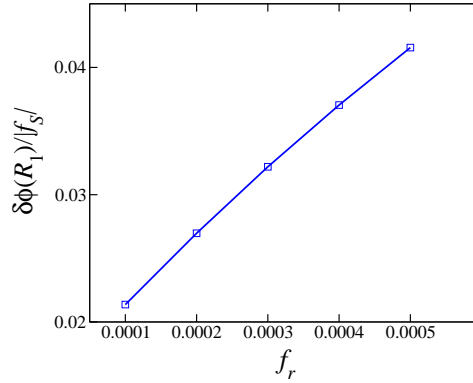


Figure 5: The f_r dependence of $\delta\phi(R_1)$. $\lambda = g = 1$, $f/M_{\text{Pl}} = 0.0002$, $R_1\omega = 2 \times 10^4$ and $h_S = (f_1 - f_S)/f = 0.005$ are fixed.

When the values of these parameters are varied, the size of the resulting lump solutions also varies. In the numerical evaluation, we have taken f and f_r in the range between 10^{-4} and 10^{-3} . In addition to these parameters, the fermion mass $m_{\text{eff}} = m - g|f_S|$ inside the lump affects the total mass (energy) of the lump.

In the numerical investigation g , λ , f , f_r , $R_1\omega$ and h_S are given to find a desired value of $\delta\phi(R_1)$ for a solution. In Fig. 4, $\delta\phi(R_1)/|f_S|$ is plotted as a function of f . From the figure it is clear that the value of the ratio $\delta\phi/|f_S|$ at R_1 is independent of f . In Fig. 5, $\delta\phi(R_1)/|f_S|$ is plotted as a function of f_r . $\delta\phi(R_1)/|f_S|$ increases as f_r increases. The numerical evaluation becomes unreliable when $\delta\phi(R_1)/|f_S|$ becomes large and the linearization in Eq. (2.8) becomes invalid. In Fig. 6, $\delta\phi(R_1)/|f_S|$ is plotted versus $R_1\omega$. As $R_1\omega$ increases, $\delta\phi(R_1)/|f_S|$ decreases and approaches a constant (~ 0.016). In Fig. 7, $\delta\phi(R_1)/|f_S|$ is plotted versus h_S . In this figure, $\delta\phi(R_1)/|f_S|$ decreases as h_S increases and

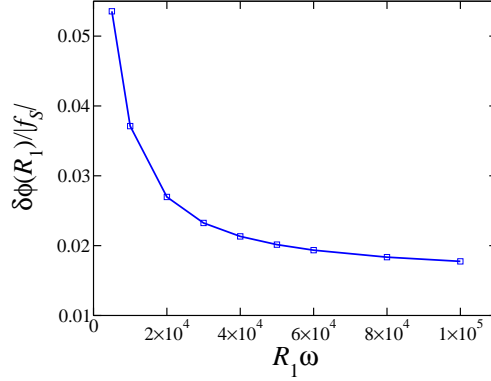


Figure 6: The R_1 dependence of $\delta\phi(R_1)$. $\lambda = g = 1$, $f/M_{\text{Pl}} = 0.0002$, $f_r = 0.0002$ and $h_S = (f_1 - f_S)/f = 0.005$ are fixed.

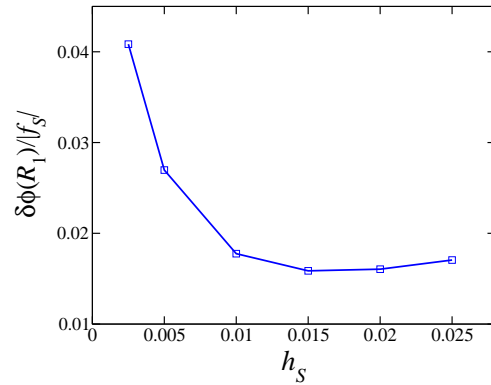


Figure 7: The h_S dependence of $\delta\phi(R_1)$. $\lambda = g = 1$, $f/M_{\text{Pl}} = 0.0002$, $f_r = 0.0002$ and $R_1\omega = 2 \times 10^4$ are fixed.

then begins to increase when h_S becomes greater than approximately 0.015. The reason for the increase in the value of $\delta\phi(R_1)/|f_S|$ is that at some point $f_1 - f_S$ becomes greater than $\delta\phi(R_1)$, which means that $\phi(R_1) < f_1$. In this situation, the solution will diverge to negative infinity if we do not take a large enough value for $\delta\phi(R_1)$.

In Figs. 8, 9, and 10, we plot the mass of the lump M as a function of f , m_{eff} , and $R_1\omega$, respectively. For the data represented in these figures, the nonrelativistic approach is justified, i.e. $p_F \ll m_{\text{eff}}$. Combining Eqs. (3.6), (3.8), (4.5), and the fact that

$$\omega^2 \sim 2\lambda f^2, \quad (5.1)$$

we may find a rough estimate of the mass of the lump

$$M \sim (-gf + m_{\text{eff}}) \left(\frac{h_S}{g\sqrt{2\lambda}} \right) \frac{4\pi(\omega R)^3}{3}. \quad (5.2)$$

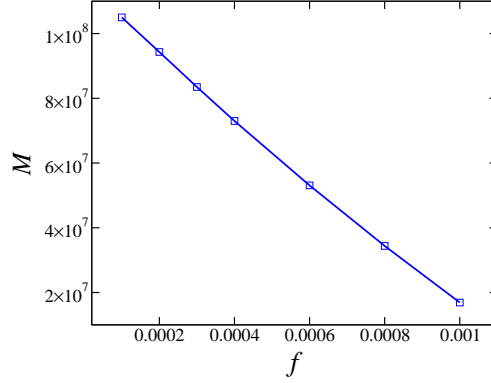


Figure 8: M versus f . $f_r = 0.0002$, $h_S = (f_1 - f_S)/f = 0.005$, $R_1\omega = 2 \times 10^4$ and $m_{\text{eff}}/M_{\text{Pl}} = 10^{-3}$ are fixed. f and M are in the units of M_{Pl} .

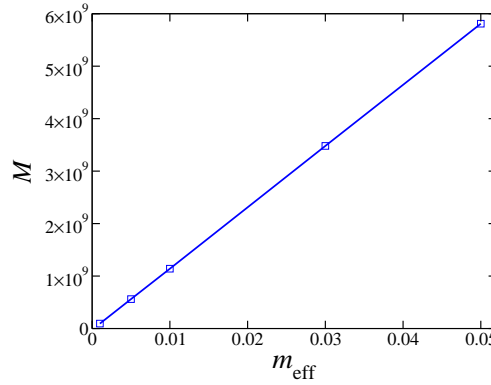


Figure 9: M versus m_{eff} . $f/M_{\text{Pl}} = 0.0002$, $f_r = 0.0002$, $h_S = 0.005$ and $R_1\omega = 2 \times 10^4$ are fixed. M and m_{eff} are in the units of M_{Pl} .

This rough estimate explains the behavior of M in Figs. 8, 9, and 10. Similarly, using Eqs. (3.6), (3.8), (4.6), (5.1), and the fact that $\rho_n \sim \pi(2\rho_0/m_{\text{eff}})^{2/3}/3$ for an ultrarelativistic Fermi gas, it is possible to find a rough estimate of the mass of a lump filled with ultrarelativistic Fermi gas

$$M \sim \left(-gf + \frac{2\pi^2\lambda}{gm_{\text{eff}}} h_S f^3 \right) \left(\frac{h_S}{g\sqrt{2\lambda}} \right) \frac{4\pi(\omega R)^3}{3}. \quad (5.3)$$

Using this equation, it is easy to extract the behavior of the lump mass M as a function of different parameters of interest.

6. Continuous transition in the boundary wall region

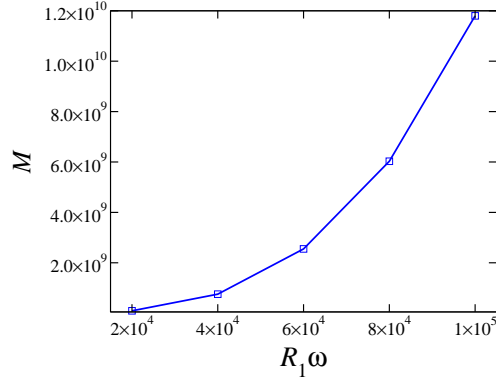


Figure 10: M versus $R_1 \omega$. $f/M_{\text{Pl}} = 0.0002$, $f_r = 0.0002$, $h_S = 0.005$ and $m_{\text{eff}}/M_{\text{Pl}} = 10^{-3}$ are fixed. M is in the units of M_{Pl} .

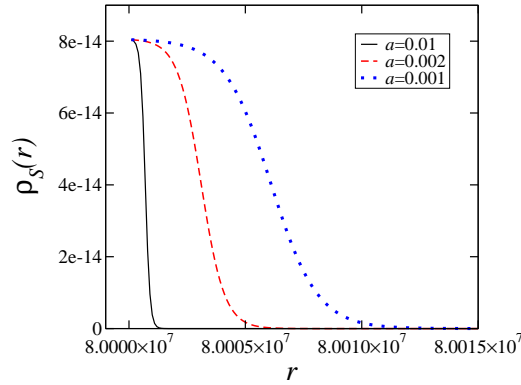


Figure 11: $\rho_S(r)$ for $a/M_{\text{Pl}} = 0.01$, $a/M_{\text{Pl}} = 0.005$ and $a/M_{\text{Pl}} = 0.001$. $R_1/l_{\text{Pl}} = 8 \times 10^7$ and $\rho_0/M_{\text{Pl}}^3 = 8.0593 \times 10^{-14}$ are fixed. ρ_S is in the units of M_{Pl}^3 .

So far we have studied the lump solutions using Eq. (2.9) to express $\rho_S(r)$. In this approximation, a small discontinuity appears in ϕ'' at $r = R_1$ due to the discontinuous change in ρ_S at this radius. In this section, we investigate the case in which ρ_S makes a continuous transition from ρ_0 to 0 in the boundary wall region (region II). To assure a smooth transition in this region, we express $\rho_S(r)$ with an equation of the form

$$\rho_S(r) = \rho_0 \left\{ 1 - \frac{1}{1 + \exp[a(R_1 - r) + 6]} \right\}. \quad (6.1)$$

This equation becomes identical to Eq. (2.9) in the limit where $a \rightarrow \infty$. In Fig. 11, we plot $\rho_S(r)$ for three different values of a . As a gets smaller, ρ_S make a slower transition from ρ_0 to zero. In Fig. 12, we show how $\delta\phi(R_1)$ decreases as we decrease the value of a . In the examples shown in Fig. 12, the transition region from $\rho_S = \rho_0$ to $\rho_S = 0$ is smaller

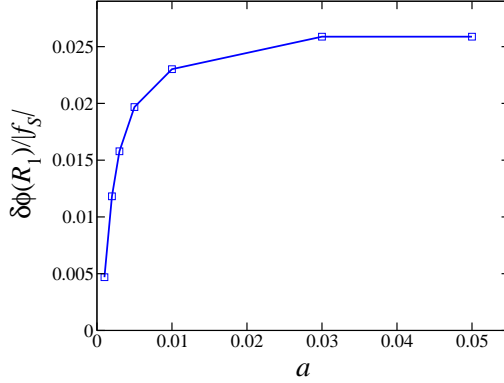


Figure 12: $\delta\phi(R_1)/|f_S|$ versus a . $f/M_{\text{Pl}} = 0.0002$, $f_r = 0.0002$, $h_S = (f_1 - f_S)/f = 0.005$ and $R_1\omega = 2 \times 10^4$ are fixed. a is in the units of M_{Pl} .

than the width $w = R_2 - R_1$. As $a \rightarrow \infty$, the value of $\delta\phi(R_1)/|f_S|$ in Fig. 12 converges to the value of $\delta\phi(R_1)/|f_S|$, which we find using the approximation in Eq. (2.9).

7. Summary and conclusions

In this paper, we have shown that false vacuum lumps with fermions in flat spacetime may exist. This configuration is an interesting configuration which may appear in different scales and masses. The size of these lumps depends on the typical energy scale of the scalar field potential. If the energy scale is very high, the size of the lump is small. If the energy scale is low, the lump may extend at a cosmic scale. On the other hand, the mass of these lumps depends both on the energy scale of the scalar potential and the mass density of fermions inside the lump. For lumps with large masses and sizes, the gravitational effects need to be included. The spacetime structure for such lumps will be de Sitter- Schwarzschild. We leave the investigation on de Sitter-Schwrschild gravitating false vacuum lumps with fermions to a future project. The stability of the solutions requires further examination as well.

False vacuum lumps with fermions are a type of non-topological soliton that may be produced in the early universe due to the spontaneous breaking of an approximate discrete symmetry that occurs in a large family of field theories in four spacetime dimensions. It has also been shown in Ref. [9] that the false vacuum lumps of the Higgs field may emerge in the early universe in the standard Einstein-Weinberg-Salam theory of electroweak and gravitational interactions. In this model, the fermions are the quarks and leptons that are

coupled with the Higgs field via Yukawa interaction. It would be interesting to study the cosmological effects and applications of such lumps.

Acknowledgments

This work was supported in part by the Natural Sciences and Engineering Research Council of Canada. I would like to thank Yutaka Hosotani for sharing his intuition and for providing invaluable assistance in the preparation of this paper.

References

- [1] I. Dymnikova, gr-qc/0010016;
- [2] R. G. Daghigh and Y. Hosotani, *Prog. Theoret. Phys.* **110** (2004) 1151, gr-qc/0307075;
- [3] R. Friedberg, T. D. Lee, and A. Sirlin, *Phys. Rev.* **D13** (1976) 2739;
- [4] T. D. Lee and Y. Pang, *Phys. Rep.* **221** (1992) 251;
- [5] S. Coleman, *Nucl. Phys.* **B262** (1985) 263;
- [6] A. L. Macpherson and B.A. Campbell, *Phys. Lett.* **B347** (1995) 205;
- [7] T. Yoshida, K. Ogure, and J. Arafune, *Phys. Rev.* **D67** (2003) 083506; *Phys. Rev.* **D68** (2003) 023519;
- [8] Y. Hosotani, T. Nakajima, R. G. Daghigh and J. I. Kapusta, *Phys. Rev.* **D66** (2002) 104020, gr-qc/0112079;
- [9] H. Emoto, Y. Hosotani, and T. Kubota, *Prog. Theoret. Phys.* **108** (2002) 157, hep-th/0201141.